Synthesis of Two-Dimensional Triazine Covalent Organic Frameworks at Ambient Conditions to Detect and Remove Water Pollutants

Maryam Salahvarzi[a], Antonio Setaro[b,c], Kai Ludwig[d], Patrick Amsalem[e], Thorsten Schultz[e,f], Ebrahim Mehdipour[a], Mohammad Nemati[a], Cheng Chong[g], Stephanie Reich[b,*], Mohsen Adeli[a*]

[a] *Department of Chemistry, Lorestan University, Khorramabad, Iran*
[b] *Department of Physics, Free University Berlin, Arnimallee 14, 14195 Berlin, Germany*
[c] *Department of Engineering, Pegaso University, Naples, Italy*
[d] *Forschungszentrum für Elektronenmikroskopie and Core Facility BioSupraMol, Institut für Chemie und Biochemie, Freie Universität Berlin, Fabeckstr. 36a, 14195 Berlin, Germany*
[e] *Institut für Physik, Humboldt-Universität zu Berlin, Newtonstr. 15, 12489 Berlin, Germany*
[f] *Helmholtz-Zentrum Berlin für Materialien und Energie GmbH, Berlin 14109, Germany*
[g] *College of Polymer Science and Engineering, State Key Laboratory of Polymer Materials Engineering, Sichuan University, Chengdu, 610065, China*
* Corresponding authors.
E-mail addresses: adeli.m@lu.ac.ir (M. Adeli), sreich@zedat.fu-berlin.de (S. Reich).

Abstract

Synthesis of fully triazine frameworks (C_3N_3) by metal catalyzed reactions at high temperatures results in carbonized and less-defined structures. Moreover, metal impurities affect the physicochemical, optical and electrical properties of the synthesized frameworks, dramatically. In this work, two-dimensional C_3N_3 ($2DC_3N_3$) has been synthesized by in situ catalyst-free copolymerization of sodium cyanide and cyanuric chloride, as cheap and commercially available precursors, at ambient conditions on gram scale. Reaction between sodium cyanide and cyanuric chloride resulted in electron-poor polyfunctional intermediates, which converted to $2DC_3N_3$ with several hundred micrometers lateral size at ambient conditions upon [2+2+2] cyclotrimerization. $2DC_3N_3$ sheets, in bulk and individually, showed strong fluorescence with 63% quantum yield and sensitive to small objects such as dyes and metal ions. The sensitivity of $2DC_3N_3$ emission to foreign objects was used to detect low concentration of water impurities. Due to the high negative surface charge (- 37.7 mV) and dispersion in aqueous solutions, they demonstrated a high potential to remove positively charged dyes from water, exemplified by excellent removal efficiency (> 99%) for methylene blue. Taking advantage of the straightforward production and strong interactions with dyes and metal ions, $2DC_3N_3$ was integrated in filters and used for the fast detection and efficient removal of water impurities.

Keywords: Covalent organic frameworks, Two-dimensional, Cyclotrimerization, Water treatment, Semiconductor, Triazine frameworks.

1. Introduction

Covalent triazine frameworks are a subset of organic polymers with a π conjugated system, exhibiting electronic effects related to nitrogen as a heteroatom in addition to high surface area and excellent chemical and thermal stability [1, 2]. Due to their peculiar electrical, optical and mechanical properties, they have attracted a great deal of attention and are currently considered for a wide range of applications including photocatalysts, semiconductors, and electrochemistry [3, 4]. Among different types of triazine frameworks, C_3N_3 is less investigated, due to a lack of available straightforward synthetic protocols [5-7]. Several procedures including solvothermal reaction of $C_3N_3Cl_3$ and NH_4Cl at 300 °C [8], $C_3N_3Cl_3$ with NaN_3 and $NaNH_2$ at 220 °C [9], solvent-free processes at 220 °C, 300 °C, and 380 °C temperatures [10], Wurtz reaction of $C_3N_3Cl_3$ in molten alkali metals [11], trimerization of 2,4,6- tricyano-1,3,5-triazine in molten $ZnCl_2$ [12], ionothermal approach [13], high pressure conditions [14], and Ullman reaction [15] have been proposed for the production of C_3N_3 frameworks [16]. However, these procedures required high temperatures and metal catalysts, leading to carbonization and metal impurities [17, 18]. Because of these issues, electronic properties of $2DC_3N_3$ are generally less studied and less information regarding their structures at atomic scale are available [19]. In order to overcome these problems and produce $2DC_3N_3$ with defined structures and reproducible physicochemical properties, new synthesis protocols using straightforward reactions at ambient conditions should be explored.

In the same line, we have reported a metal directed and solvent mediated protocol, as an alternative for the production of less defected triazine frameworks [20]. In this protocol, reaction between cyanuric chloride and calcium carbide in dimethylformamide resulted in two-dimensional triazine based nanomaterials. Coordination of calcium ions with triazine monomers was the main driving force for a two-dimensional polymerization. While this method was milder than Lewis's acid-mediated trimerization of cyanides, the temperature was still high and solvent played a role in the mechanism of reaction, leading to complexity in the obtained structure to some extent.

[2+2+2] cyclotrimerization of alkynes at ambient conditions is an important reaction in organic synthesis and bioconjugation chemistry, due to its versatility, efficiency and functional tolerance [21, 22]. It is one of the main approaches for the construction of aromatic compounds and six-membered heterocyclic rings [23-25]. The above-mentioned advantages combined with the orthogonality make this reaction an efficient strategy for the construction of complex systems in different fields including heterocyclic chemistry [26], polymer chemistry [27] and materials

science [28, 29]. However, the required catalysts increase its complexity and decrease its cost-effectiveness dramatically. Recently, we have explored a new method for the [2+2+2] polymerization of multifunctional monomers with ethynyl substituents without using any catalyst [30]. Conjugation of ethynyl segments to the electron poor triazine resulted in reactive intermediates that were susceptible to [2+2+2] cyclotrimerization, leading to triazine frameworks in a one pot reaction. The reaction was performed at room temperature and resulted in materials with several micrometers lateral size and hundred nanometer thickness. Triazine frameworks are promising platforms for the water treatment, due to their physicochemical properties [31].

Water pollutants, due to their hazardous acute and chronic effects on living systems, are challenging environmental issues around the world [32]. The largest group of pollutants are heavy metals and industrial dyes that are often toxic even at very low concentrations [33]. Industries that majorly cause water pollution are textile, pesticides, cosmetics, pharmaceutical, oil refineries, paper and pulp, paint and rubber [34]. To minimize serve effect of such pollutants on ecosystem and human health, new materials for fast and efficient water purification are highly required. Recently, insoluble and porous N-rich polymers with high surface areas, interacting favorably with other molecules through noncovalent interactions, have been used in the field of pollutant removal [35-37].

In this work, we have developed our catalyst free [2+2+2] cyclotrimerization to multifunctional monomers bearing carbonitrile substituents for the production of $2DC_3N_3$. Cyanuric chloride and sodium cyanide were incubated at 10 °C to produce reactive intermediates which were changed to $2DC_3N_3$ upon in situ cyclotrimerization at a slightly higher temperature.

The synthesized two-dimensional triazine frameworks with several micrometers' lateral sizes and negative surface charge were able to efficiently remove positively charged dyes from water. For example, 1 mg of $2DC_3N_3$ was able to separate 20 mg. L^{-1} methylene blue or Malachite green in 120 seconds. The removal efficiency for different concentrations of methylene blue and malachite green were (> 99%) and (> 90%), respectively. Moreover, $2DC_3N_3$ sheets, both in bulk and individually demonstrated a good fluorescence emission with the highest quantum yield at 360 nm that was successfully used to detect low concentrations of metal ions in water.

2. Materials and methods

The materials and methods and experimental details regarding synthesis of $2DC_3N_3$ and more information about characterizations are explained in supplementary information.

3. Results and discussion

3.1. Generation and characterization of $2DC_3N_3$

Herein, we report on a new protocol for the synthesis of $2DC_3N_3$ on gram scale from cheap and commercially available materials at ambient conditions.

Reaction between cyanuric chloride and sodium cyanide resulted in polyfunctional intermediates that were changed to $2DC_3N_3$ upon [2+2+2] cyclotrimerization (Fig. 1a). Trimerization of carbonitrile substituents was a catalyst-free reaction and mechanistically based on our recently published method for the production of covalent organic frameworks. Conjugation of carbonitrile segments to the electron poor triazine ring resulted in polarization of carbon-nitrogen triple bonds and susceptibility toward cyclotrimerization. The reaction was performed at 65 °C on gram scale without using any catalyst. The absence of carbon-nitrogen triple bond at 2200 cm^{-1} and presence of C=N absorbance band at 1540 cm^{-1} and 1350 cm^{-1} indicated the production of a covalent organic framework consisting of triazine rings through cyclotrimerization of carbonitrile functional groups (Fig. 1b). A strong absorption band at 1650 cm^{-1} and broad absorbance band at 2900-3600 cm^{-1} was assigned to the carboxyl functional groups created by hydrolyzing carbonitrile groups at the edge of $2DC_3N_3$ frameworks in the workup [38, 39]. Due to carboxyl functional groups and high negative surface charge of $2DC_3N_3$ (- 37.7 mV) and repulsion between the sheets, they were dispersible in aqueous solutions for 3 days (Fig. 1c and 1d).

AFM images demonstrated a two-dimensional structure for this compound, indicating cyclotrimerization of carbonitrile groups in two-dimensions and lateral networking of monomers in this reaction. The lateral size of $2DC_3N_3$ was large up to several micrometers with clear edges. Moreover, bulges and back-folding that are typical morphologies in two-dimensional materials were observed in the AFM images of $2DC_3N_3$ (Fig. 1e). The high dispersibility of this compound in water, due to its negative surface charge, facilitated cryo-TEM imaging to gain more information about its structure. Two-dimensional structures with several micrometers lateral size and high transparency, indicating mono or few layers, were observed abundantly (Fig. 1f and 1g). Moreover, wrinkles and folding, which are typical features for mono or few-layered two-dimensional

materials, indicated the covalent nature of their structures (movies 1 and 2) (Fig. S1 and S2). In agreement with cryo-TEM and AFM, scanning electron microscopy (SEM) revealed stacked sheet-like structures with several micrometers lateral size and clear edges (Fig. 1h and S3).

More information about the atomic structure of $2DC_3N_3$ was gained by high resolution transmission electron microscopy (HRTEM). While some of $2DC_3N_3$ sheets were completely crystalline, other were composed of crystalline domains surrounded by amorphous region (Fig. 2a). The selected area electron diffraction (SAED) pattern revealed faint diffraction rings assigned to the (002) and (200) (Fig. 2b and 2c), indicating the polycrystallinity of $2DC_3N_3$ nanosheets. This is well consistent with the sharp diffraction peak accompanied by broad shoulders in the XRD diffractogram of this compound (Fig. 4a). The distance between stacked layers of $2DC_3N_3$ sheets was 0.258 nm, in agreement with the value obtained by XRD measurements (Fig. 2d, 2e and S4). The unit cell of $2DC_3N_3$, obtained by electron diffraction pattern, was a=b=7.615 Å which is in agreement with the calculated value a=b=7.6 Å (Fig. 2f) [40]. Images indicate $2DC_3N_3$ nanosheets emerge with a planar size of 100 nm.

The composition and structure of $2DC_3N_3$ was further investigated by X-ray photoelectron spectroscopy (XPS). Based on the survey spectrum of $2DC_3N_3$ deposited on gold, it was mainly composed of carbon, nitrogen and oxygen. While nitrogen and carbon with 35% and 47% were the major components of the backbone of sheets, oxygen (17%) was assigned to the functional groups (Fig. 3a). In the C1s XPS spectrum, two peaks C1 and C2 are observed at 286.7 eV and 289.8 eV binding energy, which correspond to carbon atoms of triazine ring and carboxyl functional groups, respectively. No C-C bonds related peak is observed in the 283-285 eV range, proving thereby the minimum side reactions and the absence of other bonds than carbon-nitrogen in the backbone of $2DC_3N_3$ (Fig. 3b) [41, 42]. In the N1s XPS spectrum, two types of nitrogen atoms with their peak maximum at 398.5 eV and 401.9 eV are attributed to backbone and periphery triazine rings as shown in Fig. 3c [43].

The carbon/nitrogen (C/N) ratio of $2DC_3N_3$ measured by XPS and elemental analysis were 1.34 and 1.03 and close to calculated ratio (0.85) (Fig. 3d). The difference between the experimental and calculated C/N ratios, which was corresponding to oxygen containing functional groups, indicated minimum side reactions and preparation of a product with chemical formula shown in Fig. 1a. Three main weight losses at 100-150 °C, 350-550 °C, and 650-800 °C in TGA thermogram of $2DC_3N_3$ were corresponding to evaporation of surface moisture, detachment of functional

groups and decomposition of its backbone respectively (Fig. 3e). The thermal behavior of $2DC_3N_3$ was similar to the reported data for similar triazine frameworks in literature [44, 45]. The composition of $2DC_3N_3$ was further investigated by energy dispersive X-ray spectroscopy (EDX) elemental mapping. The homogeneous distribution of carbon, nitrogen and oxygen elements indicated a conjugated structure consisting of triazine rings accompanied by oxygen containing functional groups (Fig. 3f and S7a). The high thermal stability of $2DC_3N_3$ was corresponding to its integrated structure with minimum defects. Signal at 160 ppm in the ^{13}C solid-state cross-polarization magic-angle-spinning (CP-MAS) nuclear magnetic resonance (NMR) spectra was a further prove for the triazine backbone of the synthesized $2DC_3N_3$ (Fig. 3g). Appearing any signal in 100-140 ppm or lower chemical shifts was counted for the minimum side reactions and production of $2DC_3N_3$ with defined structure. Also shoulder at 170 ppm and a signal at 55 ppm were assigned to carbonyl and methoxy groups created by hydrolyzing carbonitrile groups and substitution of chlorides by methanol during workup, respectively [46, 47].

A sharp peak at 2θ 27° in powder X-ray diffractogram of $2DC_3N_3$ was attributed to its in-plane reflection (002) and counted for the crystalline domains of this compound (Fig. 4a) [48]. The crystalline domains were clearly observed in the high-resolution transmission electron microscopy (HRTEM) images (Fig. 2a). A weak and broadened peak centered at 2θ 41° corresponds to the vertical spacing of stacked sheets (200) in few layers $2DC_3N_3$ [49, 50]. The interlayer space of $2DC_3N_3$ sheets calculated by X-ray diffractogram was 0.253 nm.

In the same line, a broad absorption band from 225 nm to 600 nm stems from π-π* transitions of the large conjugated system of $2DC_3N_3$ (Fig. 4b and S7c) [51]. The band gap of $2DC_3N_3$ calculated by ultraviolet-visible diffused reflectance spectroscopy was 2.83 eV, which is in agreement with the reported data in literature (Fig. S7d) [52-54]. This band gap results in fluorescence emission in the range of 350-550 nm by suitable excitation in the UV and IR ranges [55]. The photoluminescence (PL) spectra of $2DC_3N_3$ in H_2O (0.5 mg. ml^{-1}) excited by different irradiations are shown in Fig. 4c. The maximum emission was achieved by excitation at longer wavelengths, 360 nm and 380 nm, indicating a large π conjugated backbone for $2DC_3N_3$. The quantum yield of $2DC_3N_3$ was 63%, which is relatively large in comparison with other similar materials [56, 57]. In order to gain more information about the fluorescence property of $2DC_3N_3$, the individual excited sheets were visualized by confocal laser scanning microscopy (CLSM) and optical microscopy.

Comparison between bright field images and CLSM images revealed that the whole backbone of $2DC_3N_3$ is emitting upon excitation by suitable wavelength (Fig. 4d, S5a and S6a).

We also incubated $2DC_3N_3$ sheets in water for several months and any significant change in their physicochemical and optical properties was not observed. This experiment indicated high stability of this material in water for a long time.

3.2. Adsorption mechanism and fluorescence emission of $2DC_3N_3$

The $2DC_3N_3$ containing triazine rings with six lone-pair electrons and high negative surface charge are excellent candidates for coordination with heavy metal ions and dye elimination by electrostatic interactions. In addition to coordination chemistry and electrostatic interactions, π–π interactions between aromatic dyes and surface of $2DC_3N_3$ is a driving force for dye removal. Such interactions between triazine platforms and metal ions and dyes is reported in literature [58].

The heavy metals such as Hg^{2+}, Cd^{2+}, Pb^{2+}, and dyes including MB and MG, are toxic for human cells even at low concentrations. Therefore, designing and synthesis of new materials with the ability of detection and removal such impurities in water, food and the environment are urgently required.

The fluorescence emission of $2DC_3N_3$ was sensitive to dyes and metal ions in terms of intensity and maximum emission wavelength (Fig. 5a-5d). The fluorescence emission of $2DC_3N_3$ in the presence of different metal ions including Cd^{2+}, Hg^{2+} and Pb^{2+} was investigated (Fig. 5a-5c). The responsivity of fluorescence emission to metal ions was different and changed upon variation of the metal ions and their concentrations. The intensity of fluorescence emission of $2DC_3N_3$ sheets increased upon addition of the metal ions but an inverse correlation was observed between the fluorescence intensity and metal ions concentrations. The highest fluorescence emission was observed at 10^{-9} M concentration of metal ions. Increasing the concentration of Cd^{2+} and Pb^{2+} to 10^{-3} M diminished their impact on the fluorescence intensity of sheets. High concentration of Hg^{2+} (10^{-3} M), however, resulted in complete quenching of sheets. The shift of maximum emission of sheets varied with the concentration of metal ions.

Moreover, addition of dyes to the water dispersion of $2DC_3N_3$ affected their emission dramatically (Fig. 5d). The responsivity of fluorescence emission of $2DC_3N_3$ to dyes was detected at 10^{-9} M concentrations. The mechanism and details for the responsivity of fluorescence of sheets to metal ions and dyes is beyond the scope of this work but can be used for detection of low concentration

of these impurities in water. A typical mechanism for sensitivity of fluorescence of these materials to metal ions is electron transfer from the excited sheets to the partially filled d-orbitals of the metal cations through the photoinduced electron transfer mechanism. Regardless of the type of metal ion, the metal chelation sites in the structure of sheets results in higher specificity and lower limit of detections [59, 60].

The emission of individual sheets in aqueous solutions (10^{-3} M) of methylene blue and Hg^{2+} was investigated (Fig. S5b and S5c). A clear quenching of the fluorescence of sheets after addition of methylene blue and Hg^{2+} was observed.

3.3. Dye adsorption performance of $2DC_3N_3$

Water contamination is one of the main challenges that affects public health worldwide. Industrial dyes are major contributors to the environmental pollution and cause severe threat to our safety and health [61, 62]. Covalent organic frameworks and two-dimensional materials with porous structure, large number of heteroatoms and high surface area, are excellent candidates for the fast and efficient absorption these impurities from wastewater [63, 64]. $2DC_3N_3$ with several micrometers lateral size and negative surface charge demonstrated a high potential to remove positively charged dyes from water, exemplified by excellent removal efficiency for methylene blue (> 99%) and malachite green (> 90%).

The ability of $2DC_3N_3$ for absorption dyes including methylene blue (MB), malachite green (MG), rhodamine B (RhB), methyl orange (MO) and congo red (CR) from water was investigated at different conditions such as incubation or sonication of their mixture in water (Fig. 6a). Sonication of a mixture of $2DC_3N_3$ (1 mg) in water removed 20 mg. L^{-1} of MG and MB in 120 seconds (Fig. 6b). In order to study the mechanism of dye adsorption, $2DC_3N_3$ (1 mg) was dispersed in 10 ml of dye solution (5-20 mg. L^{-1}) and shaken continuously for 24 h under ambient condition (25 °C). The highest adsorption capacity was measured for MB 204 mg. g^{-1} and MG 190 mg. g^{-1} (Table S2). To make the water treatment easier and faster, $2DC_3N_3$ (20 mg) was supported on a polyurethane sponge with 1cm×1cm×1cm dimensions and immersed in water containing MB (20 mg. L^{-1}). The sponge-$2DC_3N_3$ extracted dye, completely, in 120 minutes in a one-time treatment, which is fast in comparison with similar systems (Fig. 6d) [65-67]. Moreover, a filter with 2.5cm×1cm dimensions was made of sponge-$2DC_3N_3$and used to remove dyes from water (Fig. 6c). Water solutions of MB (20 mg. L^{-1}) were passed through this filter and purified water with

low dye content (> 0.01 mg. L^{-1}) was obtained. Fast filtration without needing any other treatment made this filter an excellent candidate for cost-effective water purification.

The equilibrium adsorption isotherm for dye molecules explains the interaction between adsorbent and organic dye as a function of concentration. In this study, Langmuir and Freundlich isotherm models were applied to understand the mechanism of adsorption. The linearized equation of Langmuir is represented by equation (1):

$$C_e/q_e = 1/K_L Q_m + C_e/Q_m \qquad (1)$$

Where C_e is the equilibrium dye concentration in solution (mg. L^{-1}), q_e is the amount of adsorbate adsorbed per unit weight of adsorbent (mg. g^{-1}), Q_m (mg. g^{-1}) and K_L (L. g^{-1}) are Langmuir characteristic constants, which indicate maximum adsorption capacity and adsorption energy, respectively. The values of Q_m and K_L were calculated from the slope and intercept of the linear curve C_e/q_e against C_e.

The essential characteristics of the Langmuir isotherm can be expressed in terms of a dimensionless constant separation factor R_L, which is given by the equation (2):

$$R_L = 1/1 + K_L C_0 \qquad (2)$$

Where C_0 (mg. L^{-1}) is the highest initial concentration of adsorbent and K_L (L. g^{-1}) is the Langmuir constant. R_L values indicate whether the process is unfavorable ($R_L > 1$), linear ($R_L = 1$), favorable ($0 < R_L < 1$), or irreversible ($R_L = 0$) [68].

The Freundlich equation is given by:

$$lnq_e = lnK_F + 1/n \; lnC_e \qquad (3)$$

Where, q_e (mg. g^{-1}) is the amount of adsorbate adsorbed on per unit weight of adsorbent, C_e (mg. L^{-1}) is the equilibrium dye concentration in solution, K_F ($mg^{1-1/n}$. $L^{1/n}$. g^{-1}) and 1/n are the Freundlich characteristic constants representing adsorption capacity and adsorption intensity, respectively [69]. The values of K_F and 1/n were computed from the intercept and slope of the linear curve Ln q_e against Ln C_e. When n is equal to 1, the adsorption is linear. Additional, n below unity shows that adsorption is a chemical, while above unity indicates a physical process [70, 71]. Correlation coefficient (R^2) of Freundlich isotherm model for adsorption of MB and MG by $2DC_3N_3$ was bigger than that of the Langmuir isotherm model and almost equal to unity, thus suitable for the prediction of adsorption capacity of this covalent organic framework (Fig. 6e and 6f). Fitting parameters for both models are summarized in Table S1. Based on the Freundlich model, dyes were adsorbed heterogeneously on the surface of $2DC_3N_3$ [72]. According to this

model, adsorption sites have different energy values and active adsorption locations possessing maximum energy are filled at first, causing the fast uptake and high adsorption capacity of MB and MG by $2DC_3N_3$. The heterogeneous adsorption of MB on $2DC_3N_3$ was observed by CLSM and optical microscopy (Fig. S5c and S6b).

Fig. 7a shows the influence of contact time on MB and MG adsorption at different concentrations. The adsorption capacity increased rapidly within 90 min, and then increased gradually until equilibrium reached within 270 minutes. Kinetic studies could describe the relationship between the adsorption capacity and time. Additionally, it provides information about the adsorption mechanism and rate-controlling adsorption steps [73, 74].

For this reason, experimental data were adjusted with the pseudo-first-order (4) and pseudo-second-order (5) kinetic models [75]:

$$log(q_e - q_t) = logq_e - K_1\, t/2.303 \qquad (4)$$

$$t/q_t = 1/K_2 q_e^2 + t/q_e \qquad (5)$$

Where K_1 and K_2 were the rate constants of the pseudo-first-order and pseudo-second order (g. mg^{-1}. min^{-1}) kinetic models, respectively, and t was the adsorption time (min).

The pseudo-first-order and pseudo-second-order kinetic parameters including R^2, K_1, K_2, calculated q_e ($q_{e,cal}$) and experimental q_e ($q_{e,exp}$) are presented in Table S2. The kinetic data for adsorption of MB and MG by $2DC_3N_3$ were fitted with pseudo-first-order model, indicating dependency of the kinetic of dye adsorption to the dye concentration (Fig. 7b and 7c).

3.4. The effect of solution pH

The pH value of the dye solution plays an important role in the adsorption process. By controlling the pH value of the dye solution, the effect of electrostatic interaction on the adsorption of dye can be explored [76-78]. Fig. 8a shows the effects of the solution pH on the adsorption capacity of $2DC_3N_3$. The results indicate that there is a significant difference between adsorption capacities of $2DC_3N_3$ at different pHs. The adsorption capacity of $2DC_3N_3$ for MB and MG amplifies with increased pH in the range of 2-9. Protonation of $2DC_3N_3$ at low pHs decreases its surface charge and diminishes its interactions with positively charged MB and MG. However, at alkaline conditions, the surface charge of $2DC_3N_3$ was highly negative and adsorbed positively charged dyes by electrostatic interactions (Fig. S7b) [79, 80].

Desorption processes aiming to recover matrices and pollutants are important to reduce the cost of an industrial process as well as the environmental impact [81, 82]. Therefore, we studied the reusability of the adsorbent for three consecutive adsorption-desorption cycles. As shown in Fig. 8b, the adsorption efficiency of MB and MG was almost same in the three cycles, indicating that $2DC_3N_3$ can be used repeatedly for the removal of mentioned dyes.

$2DC_3N_3$ sheets, due to their outstanding physical and chemical properties demonstrated remarkable potential for the fast and efficient absorption of impurities from the contaminated water. Finding an effective, low-cost, stable and flexible strategy for detection and removing water impurities is a challenge in the whole world. Filtration technologies may solve many problems related to low water quality, but are limited by their effectiveness cost, and accessibility. Nevertheless, most of these strategies still suffer from various drawbacks such as secondary pollution, complex operation process and expensive installation costs [83].

Metal and dye separation with $2DC_3N_3$-based filters is considered one of the prominent methods due to its convenient operation, low-cost, energy and time saving, and environmental friendliness and repeated use without flux reduction [84].

4. Conclusion

In this work, we have demonstrated the successful one-pot synthesis of two-dimensional triazine frameworks by reaction between cyanuric chloride and sodium cyanide at mild conditions. Catalyst-free [2+2+2] cyclotrimerization of carbonitrile functional groups conjugated to triazine ring at low temperature resulted in large triazine sheets up to several hundred micrometers lateral size with an intense fluorescence emission. Due to the presence of heteroatoms and negative surface charge, $2DC_3N_3$ sheets were able to efficiently adsorbed metal ions and positively charged dyes from aqueous solutions. The sensitivity of fluorescence of sheets to low concentrations of metal ions and dyes was used to detect these impurities. Cost-effective synthetic protocol and efficient dye removal together with the flexible applicability, exemplified by sponge-$2DC_3N_3$, makes this two-dimensional polymer an excellent candidate for water purification and other applications related to environmental safety.

Acknowledgment

We would like to thank Iran Science Elites Federation and Iran National Science Foundation (Project Number 4001281) for the financial support.

References

[1] C. Wang, P. Lyu, Z. Chen, Y. Xu, Green and Scalable Synthesis of Atomic-Thin Crystalline Two-Dimensional Triazine Polymers with Ultrahigh Photocatalytic Properties, Journal of the American Chemical Society (**2023**).
[2] M.G. Mohamed, A.F. El-Mahdy, Y. Takashi, S.-W. Kuo, Ultrastable conductive microporous covalent triazine frameworks based on pyrene moieties provide high-performance CO 2 uptake and supercapacitance, New Journal of Chemistry 44(20) (**2020**) 8241-8253.
[3] H. Wang, H. Wang, Z. Wang, L. Tang, G. Zeng, P. Xu, M. Chen, T. Xiong, C. Zhou, X. Li, Covalent organic framework photocatalysts: structures and applications, Chemical Society Reviews 49(12) (**2020**) 4135-4165.
[4] H. Zhu, W.D. Wang, F. Li, X. Sun, B. Li, Q. Song, J. Kou, K. Ma, X. Ren, Z. Dong, Facile preparation of ultrafine Pd nanoparticles anchored on covalent triazine frameworks catalysts for efficient N-alkylation, Journal of Colloid and Interface Science 606 (**2022**) 1340-1351.
[5] S. Kumar, V.R. Battula, K. Kailasam, Single molecular precursors for CxNy materials-Blending of carbon and nitrogen beyond g-C3N4, Carbon 183 (**2021**) 332-354.
[6] H. Yang, Z. Wang, S. Liu, Y. Shen, Y. Zhang, Molecular engineering of CxNy: topologies, electronic structures and multidisciplinary applications, Chinese Chemical Letters 31(12) (**2020**) 3047-3054.
[7] B. Antil, S. Deka, Porous Graphitic Carbon Nitride Nanostructures and Their Application in Photocatalytic Hydrogen Evolution Reaction, Heterogeneous Nanocatalysis for Energy and Environmental Sustainability 1 (**2022**) 133-163.
[8] N. López-Salas, J. Albero, CxNy: new carbon nitride organic photocatalysts, Frontiers in Materials 8 (**2021**) 772200.
[9] Y. Kojima, H. Ohfuji, Reexamination of solvothermal synthesis of layered carbon nitride, Journal of Materials 2018 (**2018**).
[10] C.-Y. Wang, K. Maeda, L.-L. Chang, K.-L. Tung, C. Hu, Synthesis and applications of carbon nitride (CNx) family with different carbon to nitrogen ratio, Carbon 188 (**2022**) 482-491.
[11] H. Yin, Q. Guo, D. He, J. Li, S. Sun, Structural characterization and electrochemical performance of macroporous graphite-like C 3 N 3 prepared by the wurtz reaction and heat treatment, RSC advances 7(69) (**2017**) 44001-44008.
[12] J. Zeng, Z. Chen, X. Zhao, W. Yu, S. Wu, J. Lu, K.P. Loh, J. Wu, From all-triazine C3N3 framework to nitrogen-doped carbon nanotubes: efficient and durable trifunctional electrocatalysts, ACS Applied Nano Materials 2(12) (**2019**) 7969-7977.
[13] Z.A. Lan, M. Wu, Z. Fang, Y. Zhang, X. Chen, G. Zhang, X. Wang, Ionothermal Synthesis of Covalent Triazine Frameworks in a NaCl-KCl-ZnCl2 Eutectic Salt for the Hydrogen Evolution Reaction, Angewandte Chemie International Edition 61(18) (**2022**) e202201482.
[14] S. Fanetti, M.M. Nobrega, K. Dziubek, M. Citroni, A. Sella, P.F. McMillan, M. Hanfland, R. Bini, Structure and reactivity of 2, 4, 6-tricyano-1, 3, 5-triazine under high-pressure conditions, CrystEngComm 21(30) (**2019**) 4493-4500.
[15] J. Feng, M. Li, Large-scale synthesis of a new polymeric carbon nitride—C3N3 with good photoelectrochemical performance, Advanced Functional Materials 30(23) (**2020**) 2001502.

[16] Y.-M. Li, L. Yang, L. Sun, L. Ma, W.-Q. Deng, Z. Li, Chemical fixation of carbon dioxide catalyzed via covalent triazine frameworks as metal free heterogeneous catalysts without a cocatalyst, Journal of Materials Chemistry A 7(45) (**2019**) 26071-26076.
[17] D. Vidyasagar, T. Bhoyar, G. Singh, A. Vinu, Recent progress in polymorphs of carbon nitride: Synthesis, properties, and their applications, Macromolecular Rapid Communications 42(7) (**2021**) 2000676.
[18] M. Liu, X. Wang, J. Liu, K. Wang, S. Jin, B. Tan, Palladium as a superior cocatalyst to platinum for hydrogen evolution using covalent triazine frameworks as a support, ACS applied materials & interfaces 12(11) (**2020**) 12774-12782.
[19] M.G. Mohamed, A.F. EL-Mahdy, M.G. Kotp, S.-W. Kuo, Advances in porous organic polymers: Syntheses, structures, and diverse applications, Materials Advances 3(2) (**2022**) 707-733.
[20] A. Faghani, M.F. Gholami, M. Trunk, J. Müller, P. Pachfule, S. Vogl, I. Donskyi, M. Li, P. Nickl, J. Shao, Metal-assisted and solvent-mediated synthesis of two-dimensional triazine structures on Gram Scale, Journal of the American Chemical Society 142(30) (**2020**) 12976-12986.
[21] R. Kulkarni, J. Huang, M. Trunk, D. Burmeister, P. Amsalem, J. Müller, A. Martin, N. Koch, D. Kass, M.J. Bojdys, Direct growth of crystalline triazine-based graphdiyne using surface-assisted deprotection–polymerisation, Chemical Science 12(38) (**2021**) 12661-12666.
[22] T. Nagata, Y. Obora, Transition-Metal-Mediated/Catalyzed Synthesis of Pyridines, Pyrimidines, and Triazines by [2+ 2+ 2] Cycloaddition Reactions, Asian Journal of Organic Chemistry 9(10) (**2020**) 1532-1547.
[23] A. Sen, T. Sato, A. Ohno, H. Baek, A. Muranaka, Y.M. Yamada, Polymer-Supported-Cobalt-Catalyzed Regioselective Cyclotrimerization of Aryl Alkynes, JACS Au 1(11) (**2021**) 2080-2087.
[24] K. Cen, M. Usman, W. Shen, M. Liu, R. Yang, J. Cai, A review on the assembly of multi-substituted pyridines via Co-catalyzed [2+ 2+ 2] cycloaddition with nitriles, Organic & Biomolecular Chemistry 20(37) (**2022**) 7391-7404.
[25] M. Babazadeh, S. Soleimani-Amiri, E. Vessally, A. Hosseinian, L. Edjlali, Transition metal-catalyzed [2+ 2+ 2] cycloaddition of nitrogen-linked 1, 6-diynes: a straightforward route to fused pyrrolidine systems, RSC advances 7(69) (**2017**) 43716-43736.
[26] G. Lin, M. Duan, J.M. Perez-Aguilar, Z. Gu, Y. Tu, Mild adsorption of carbon nitride (C3N3) nanosheet on a cellular membrane reveals its suitable biocompatibility, Colloids and Surfaces B: Biointerfaces 205 (**2021**) 111896.
[27] J. Zhu, C. Yang, C. Lu, F. Zhang, Z. Yuan, X. Zhuang, Two-dimensional porous polymers: from sandwich-like structure to layered skeleton, Accounts of chemical research 51(12) (**2018**) 3191-3202.
[28] Y. Xu, R.S. Sprick, N.J. Brownbill, F. Blanc, Q. Li, J.W. Ward, S. Ren, A.I. Cooper, Bottom-up wet-chemical synthesis of a two-dimensional porous carbon material with high supercapacitance using a cascade coupling/cyclization route, Journal of Materials Chemistry A 9(6) (**2021**) 3303-3308.
[29] Ò. Torres, M. Fernàndez, À. Díaz-Jiménez, A. Pla-Quintana, A. Roglans, M. Solà, Examining the factors that govern the regioselectivity in rhodium-catalyzed alkyne cyclotrimerization, Organometallics 38(14) (**2019**) 2853-2862.
[30] Salahvarzi M, Setaro A, Nemati M, Gordeev G , Fiebor A, Ludwig K , Nasiri N, Beyranvand S, Ahmadi V, Weber M, Satari Sh, Jamshidie Z, Chong Ch, Reich S, Adelia M. Constructing

covalent organic frameworks via catalyst-free alkyne trimerization at room temperature for the fast water treatment. (**2023)**
[31] A.A. Aslam, A. Irshad, M.S. Nazir, M. Atif, A review on covalent organic frameworks as adsorbents for organic pollutants, Journal of Cleaner Production (**2023**) 136737.
[32] F. Kordbacheh, G. Heidari, Water Pollutants and Approaches for their Removal, Materials Chemistry Horizons 2(2) (**2023**) 139-153.
[33] A. Elgarahy, K. Elwakeel, S. Mohammad, G. Elshoubaky, A critical review of biosorption of dyes, heavy metals and metalloids from wastewater as an efficient and green process, Cleaner Engineering and Technology 4 (**2021**) 100209.
[34] G. Palani, A. Arputhalatha, K. Kannan, S.K. Lakkaboyana, M.M. Hanafiah, V. Kumar, R.K. Marella, Current trends in the application of nanomaterials for the removal of pollutants from industrial wastewater treatment—a review, Molecules 26(9) (**2021**) 2799.
[35] R. Ghanbari, N. Amanat, Approaches of membrane modification for water treatment, Materials Chemistry Horizons 1(3) (**2022**) 153-167.
[36] J. Ghanbari, A. Mobinikhaledi, Synthesis and characterization of a novel N-rich porous organic polymer and its application as an efficient porous adsorbent for the removal of Pb (II) and Cd (II) ions from aqueous solutions, Environmental Science and Pollution Research 30(26) (**2023**) 68919-68933.
[37] H. Shan, S. Li, Z. Yang, X. Zhang, Y. Zhuang, Q. Zhu, D. Cai, P. Qin, J. Baeyens, Triazine-based N-rich porous covalent organic polymer for the effective detection and removal of Hg (II) from an aqueous solution, Chemical Engineering Journal 426 (**2021**) 130757.
[38] N. Yang, Y. Gu, Y. Shan, C. Tian, L. Yang, H. Jiang, H. Liu, X. Zhu, S. Dai, Dual rate-modulation approach for the preparation of crystalline covalent triazine frameworks displaying efficient sodium storage, ACS Macro Letters 11(1) (**2021**) 60-65.
[39] W. Wang, W. Dong, L. Ji, Y. Xia, S. Yang, Solubility of graphene-like two-dimensional layered C 3 N 3, Chemical Communications 58(100) (**2022**) 13971-13974.
[40] S. SARIKURT, F. ERSAN, Phononic stability analysis of two-dimensional carbon nitride monolayers, Marmara Fen Bilimleri Dergisi 30(4) (**2018**) 383-387.
[41] A.I. Large, S. Wahl, S. Abate, I. da Silva, J.J. Delgado Jaen, N. Pinna, G. Held, R. Arrigo, Investigations of carbon nitride-supported Mn3O4 oxide nanoparticles for ORR, Catalysts 10(11) (**2020**) 1289.
[42] Y. Noda, C. Merschjann, J. Tarábek, P. Amsalem, N. Koch, M.J. Bojdys, Directional Charge Transport in Layered Two-Dimensional Triazine-Based Graphitic Carbon Nitride, Angewandte Chemie International Edition 58(28) (**2019**) 9394-9398.
[43] Z. Yang, H. Chen, S. Wang, W. Guo, T. Wang, X. Suo, D.-e. Jiang, X. Zhu, I. Popovs, S. Dai, Transformation strategy for highly crystalline covalent triazine frameworks: from staggered AB to eclipsed AA stacking, Journal of the American Chemical Society 142(15) (**2020**) 6856-6860.
[44] W. Niu, Y. Yang, Graphitic carbon nitride for electrochemical energy conversion and storage, ACS Energy Letters 3(11) (**2018**) 2796-2815.
[45] B.P. Mathew, Z. Khan, Graphitic carbon nitride/polymer nanocomposites, Synthesis, Characterization, and Applications of Graphitic Carbon Nitride, Elsevier (**2023**) 77-110.
[46] Z. Qian, Z.J. Wang, K.A. Zhang, Covalent triazine frameworks as emerging heterogeneous photocatalysts, Chemistry of Materials 33(6) (**2021**) 1909-1926.
[47] G. Zhou, Y. Shan, Y. Hu, X. Xu, L. Long, J. Zhang, J. Dai, J. Guo, J. Shen, S. Li, Half-metallic carbon nitride nanosheets with micro grid mode resonance structure for efficient photocatalytic hydrogen evolution, Nature communications 9(1) (**2018**) 3366.

[48] Z. Li, J. Feng, J. Cao, J. Jin, Y. Zhou, D. Cao, Z. Liang, B. Zhu, M. Li, L. Zhao, New carbon nitride C3N3 additive for improving cationic defects of perovskite solar cells, Energy & Environmental Materials 6(1) (**2023**) e12283.
[49] M. Inagaki, T. Tsumura, T. Kinumoto, M. Toyoda, Graphitic carbon nitrides (g-C3N4) with comparative discussion to carbon materials, Carbon 141 (**2019**) 580-607.
[50] V. Lakshmi, C.-H. Liu, M. Rajeswara Rao, Y. Chen, Y. Fang, A. Dadvand, E. Hamzehpoor, Y. Sakai-Otsuka, R.S. Stein, D.F. Perepichka, A two-dimensional poly (azatriangulene) covalent organic framework with semiconducting and paramagnetic states, Journal of the American Chemical Society 142(5) (**2020**) 2155-2160.
[51] Y. Pan, D. Li, H.L. Jiang, Sodium-Doped C3N4/MOF Heterojunction Composites with Tunable Band Structures for Photocatalysis: Interplay between Light Harvesting and Electron Transfer, Chemistry–A European Journal 24(69) (**2018**) 18403-18407.
[52] A. Chaves, J.G. Azadani, H. Alsalman, D. Da Costa, R. Frisenda, A. Chaves, S.H. Song, Y.D. Kim, D. He, J. Zhou, Bandgap engineering of two-dimensional semiconductor materials, npj 2D Materials and Applications 4(1) (**2020**) 29.
[53] Y. Wang, L. Wang, X. Zhang, X. Liang, Y. Feng, W. Feng, Two-dimensional nanomaterials with engineered bandgap: Synthesis, properties, applications, Nano Today 37 (**2021**) 101059.
[54] D. Schwarz, Y.S. Kochergin, A. Acharjya, A. Ichangi, M.V. Opanasenko, J. Čejka, U. Lappan, P. Arki, J. He, J. Schmidt, Tailored Band Gaps in Sulfur-and Nitrogen-Containing Porous Donor–Acceptor Polymers, Chemistry–A European Journal 23(53) (**2017**) 13023-13027.
[55] N.A.M. Razali, W.N.W. Salleh, F. Aziz, A.F. Ismail, W.M.A.W. Mahmood, Graphitic Carbon Nitride (gC 3 N 4)-Based Photocatalysts for Wastewater Treatment, Advanced Materials for Wastewater Treatment and Desalination (**2022**) 1.
[56] Y. Wang, Q. Zhang, X.-Z. Li, Z. Shu, Y. Zhang, C. Gao, Y. Li, H. Liu, C. Li, H.-H. Fang, Highly Fluorescent Semiconducting Two-Dimensional Conjugated Polymer Films Achieved by Side-Chain Engineering Showing Large Exciton Diffusion Length, CCS Chemistry (**2022**) 1-12.
[57] A. Hayat, M. Sohail, A. El Jery, K.M. Al-Zaydi, S. Raza, J. Khan, H. Ali, Z. Ajmal, T. Taha, I. Ud Din, Different Dimensionalities, Morphological Advancements and Engineering of g-C3N4-Based nanomaterials for Energy Conversion and Storage, The Chemical Record (**2023**) e202200171.
[58] X. Wang, X. Li, J. Wang, H. Zhu, Recent advances in carbon nitride-based nanomaterials for the removal of heavy metal ions from aqueous solution, J. Inorg. Mater 35(3) (**2020**).
[59] T. Skorjanc, D. Shetty, M. Valant, Covalent organic polymers and frameworks for fluorescence-based sensors, ACS sensors 6(4) (**2021**) 1461-1481.
[60] D. Shetty, S. Boutros, A. Eskhan, A.M. De Lena, T. Skorjanc, Z. Asfari, H. Traboulsi, J. Mazher, J. Raya, F. Banat, Thioether-crown-rich calix [4] arene porous polymer for highly efficient removal of mercury from water, ACS applied materials & interfaces 11(13) (**2019**) 12898-12903.
[61] R. Al-Tohamy, S.S. Ali, F. Li, K.M. Okasha, Y.A.-G. Mahmoud, T. Elsamahy, H. Jiao, Y. Fu, J. Sun, A critical review on the treatment of dye-containing wastewater: Ecotoxicological and health concerns of textile dyes and possible remediation approaches for environmental safety, Ecotoxicology and Environmental Safety 231 (**2022**) 113160.
[62] Y. Sun, Y. Li, X. Zhang, J. Duan, J. Dong, J. Peng, J. Sun, S. Ai, J. Hou, Confined synthesis of g-C3N4 modified porous carbons for efficient removal of Cd ions, Science of The Total Environment (**2023**) 164167.

[63] C. Arqueros, F. Zamora, C. Montoro, A perspective on the application of covalent organic frameworks for detection and water treatment, Nanomaterials 11(7) (**2021**) 1651.
[64] Y.-C. Hsu, M.C. Sil, C.-H. Lin, C.-M. Chen, Modification of covalent organic framework by hydrolysis for efficient and selective removal of organic dye, Applied Surface Science 612 (**2023**) 155890.
[65] X. Shi, D. Ma, F. Xu, Z. Zhang, Y. Wang, Table-salt enabled interface-confined synthesis of covalent organic framework (COF) nanosheets, Chemical Science 11(4) (**2020**) 989-996.
[66] N. Basel, Q. Liu, L. Fan, Q. Wang, N. Xu, Y. Wan, Q. Dong, Z. Huang, T. Guo, Surface charge enhanced synthesis of TpEB-based covalent organic framework (COF) membrane for dye separation with three typical charge properties, Separation and Purification Technology 303 (**2022**) 122243.
[67] M. Zeng, M. Chen, D. Huang, S. Lei, X. Zhang, L. Wang, Z. Cheng, Engineered two-dimensional nanomaterials: An emerging paradigm for water purification and monitoring, Materials Horizons 8(3) (**2021**) 758-802.
[68] S. Han, K. Liu, L. Hu, F. Teng, P. Yu, Y. Zhu, Superior adsorption and regenerable dye adsorbent based on flower-like molybdenum disulfide nanostructure, Scientific reports 7(1) (**2017**) 43599.
[69] Y. Zhang, X. Hong, X.-M. Cao, X.-Q. Huang, B. Hu, S.-Y. Ding, H. Lin, Functional porous organic polymers with conjugated triaryl triazine as the core for superfast adsorption removal of organic dyes, ACS Applied Materials & Interfaces 13(5) (**2021**) 6359-6366.
[70] M.J. Pirouz, M.H. Amini, M.H. Beyki, Chromium-based covalent coordination nano-polymer: a promising dye elimination compound for water purification, Desalin Water Treat 227 (**2021**) 360-369.
[71] S.-X. Xu, Z.-Q. Yao, Y.-H. Zhang, A covalent organic framework exhibiting amphiphilic selective adsorption toward ionic organic dyes tuned by pH value, European Polymer Journal 133 (**2020**) 109764.
[72] L. Wang, Y. Tao, J. Wang, M. Tian, S. Liu, T. Quan, L. Yang, D. Wang, X. Li, D. Gao, A novel hydroxyl-riched covalent organic framework as an advanced adsorbent for the adsorption of anionic azo dyes, Analytica Chimica Acta 1227 (**2022**) 340329.
[73] Y. Song, J. Phipps, C. Zhu, S. Ma, Porous Materials for Water Purification, Angewandte Chemie International Edition 62(11) (**2023**) e202216724.
[74] Y. Liu, Y. Cui, C. Zhang, J. Du, S. Wang, Y. Bai, Z. Liang, X. Song, Post-cationic modification of a pyrimidine-based conjugated microporous polymer for enhancing the removal performance of anionic dyes in water, Chemistry–A European Journal 24(29) (**2018**) 7480-7488.
[75] H. Zhang, X. Shi, J. Li, P. Kumar, B. Liu, Selective dye adsorption by zeolitic imidazolate framework-8 loaded UiO-66-NH2, Nanomaterials 9(9) (**2019**) 1283.
[76] J. Liu, G. Li, Y. Yu, X. Zhou, Hierarchically porous covalent organic framework for adsorption and removal of triphenylmethane dyes, Microporous and Mesoporous Materials 312 (**2021**) 110703.
[77] S. Karak, K. Dey, A. Torris, A. Halder, S. Bera, F. Kanheerampockil, R. Banerjee, Inducing disorder in order: hierarchically porous covalent organic framework nanostructures for rapid removal of persistent organic pollutants, Journal of the American Chemical Society 141(18) (**2019**) 7572-7581.
[78] J. Wu, J. Liu, B. Wen, Y. Li, B. Zhou, Z. Wang, S. Yang, R. Zhao, Nitrogen-rich covalent triazine frameworks for high-efficient removal of anion dyes and the synergistic adsorption of cationic dyes, Chemosphere 272 (**2021**) 129622.

[79] Y. Li, C.-X. Yang, H.-L. Qian, X. Zhao, X.-P. Yan, Carboxyl-functionalized covalent organic frameworks for the adsorption and removal of triphenylmethane dyes, ACS Applied Nano Materials 2(11) (**2019**) 7290-7298.
[80] Y. He, X. Fu, B. Li, H. Zhao, D. Yuan, B. Na, Highly Efficient Organic Dyes Capture Using Thiol-Functionalized Porous Organic Polymer, ACS omega 7(21) (**2022**) 17941-17947.
[81] E. Saputra, B.A. Prawiranegara, H. Sugesti, M.W. Nugraha, P.S. Utama, Covalent triazine framework: Water treatment application, Journal of Water Process Engineering 48 (**2022**) 102874.
[82] F. An, J. Liu, Z. Xu, S. Zheng, Efficient removal of three dyes using porous covalent triazine frameworks: Adsorption mechanism and role of pore distribution, Water Science and Technology 82(12) (**2020**) 3023-3031.
[83] Y. Ge, Z. Li, Application of lignin and its derivatives in adsorption of heavy metal ions in water: a review, ACS Sustainable Chemistry & Engineering 6(5) (**2018**) 7181-7192.
[84] Z. Ma, X. Zhao, Q. Tang, Z. Zhou, Computational prediction of experimentally possible g-C3N3 monolayer as hydrogen purification membrane, International journal of hydrogen energy 39(10) (**2014**) 5037-5042.

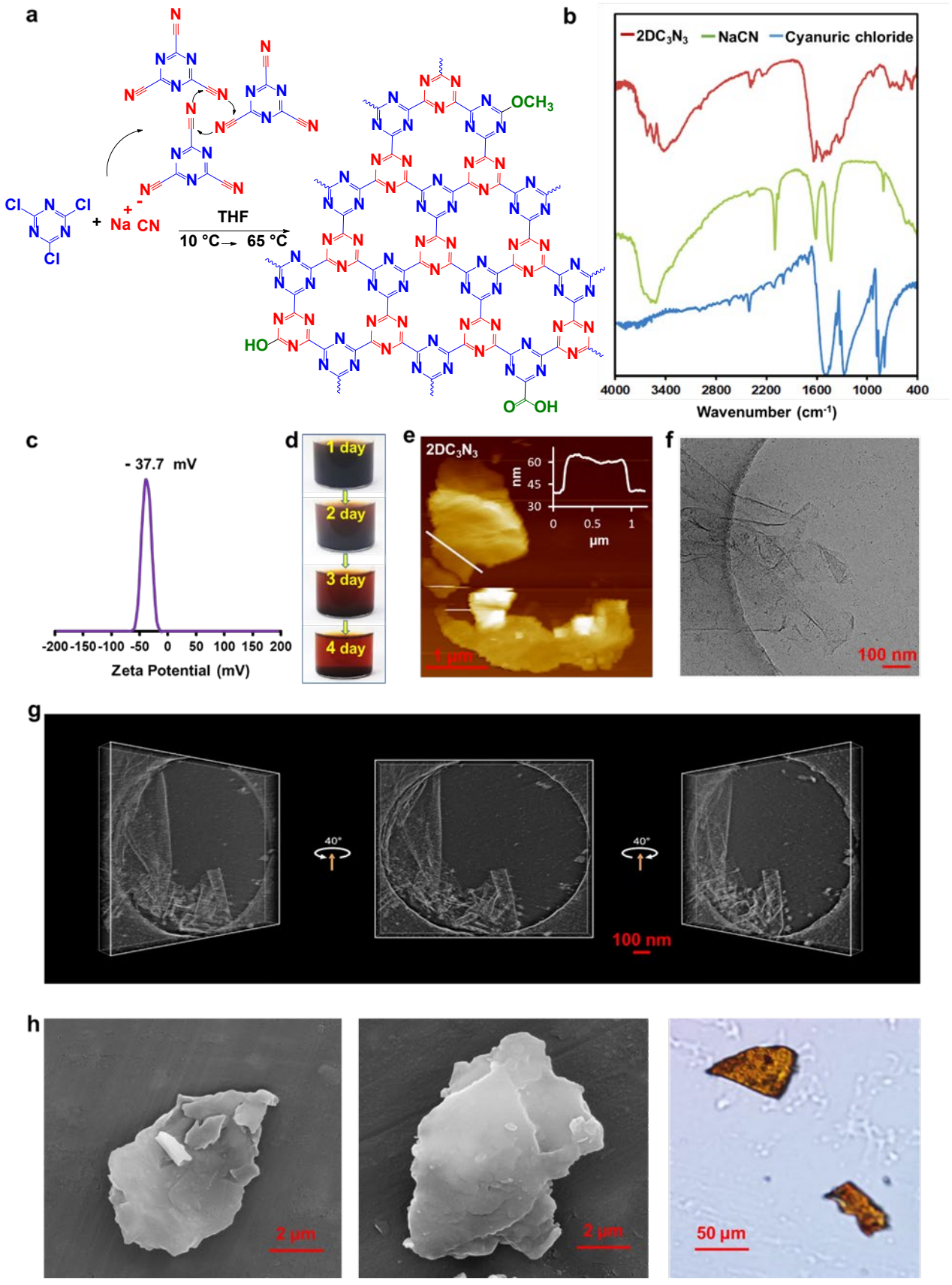
a
THF
10 °C → 65 °C
b
2DC3N3
NaCN
Cyanuric chloride
4000 3400 2800 2200 1600 1000 400
Wavenumber (cm-1)
c
- 37.7 mV
-200 -150 -100 -50 0 50 100 150 200
Zeta Potential (mV)
d
1 day
2 day
3 day
4 day
e
2DC3N3
60
45
30
nm
0 0.5 1
μm
1 μm
f
100 nm
g
40°
40°
100 nm
h
2 μm
2 μm
50 μm

Fig. 1. (a) Schematic representation of the synthesis of $2DC_3N_3$. (b) IR spectra of $2DC_3N_3$ and its precursors. (c) Zeta potential curve of $2DC_3N_3$ (1 mg. ml^{-1}) indicating a high negative surface charge for this compound in aqueous solutions. (d) Digital photographs of an aqueous solution (2 mg. ml^{-1}) of $2DC_3N_3$ at room temperature and ambient conditions for four days. (e) AFM image of $2DC_3N_3$ sheets with clear edges. (f) Cryo-TEM image of $2DC_3N_3$, displaying transparent sheets with several micrometer lateral size. (g) Voltex presentation of a 3D volume of a vitrified sample of $2DC_3N_3$ obtained by cryo-ET. The figure illustrates that the sheets fold back or partially rolls up in water. (h) SEM and optical microscopy images of $2DC_3N_3$ sheets.

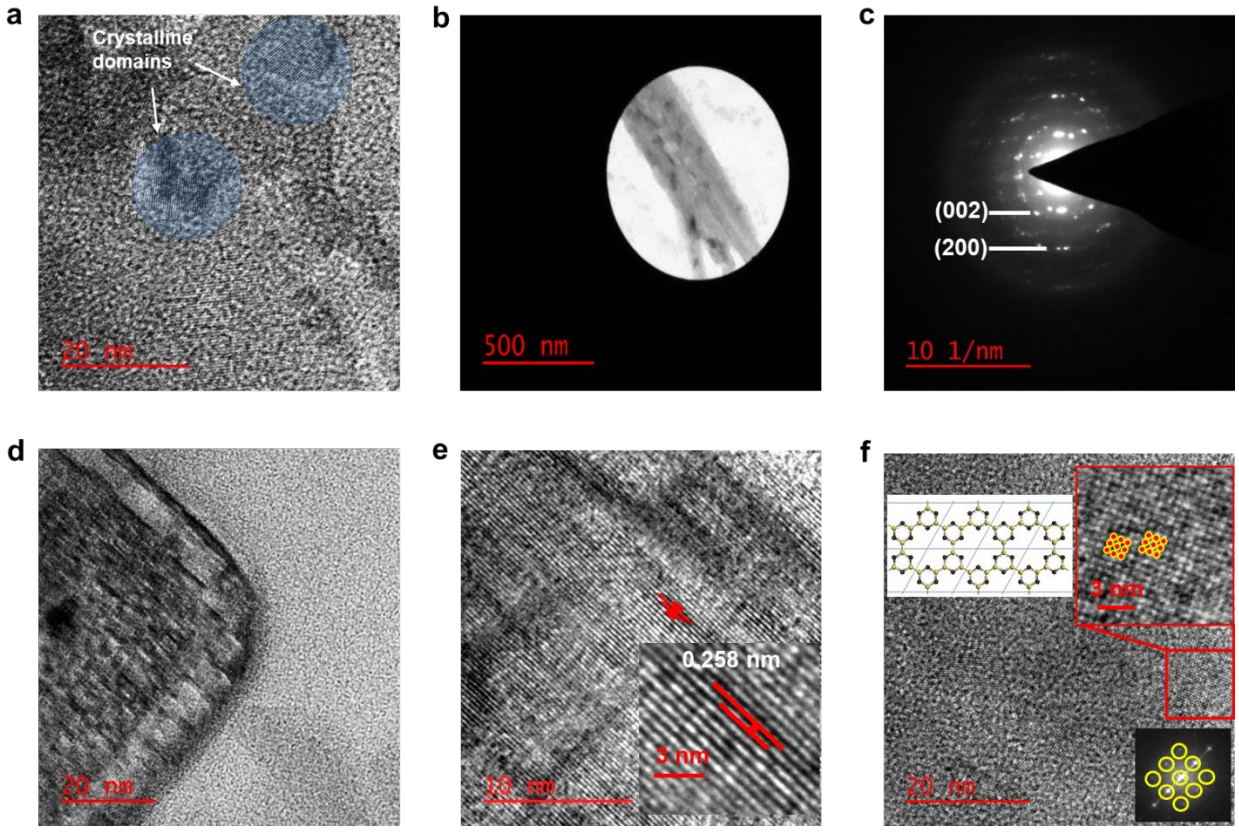

Fig. 2. (a) HRTM image of a $2DC_3N_3$ sheet, showing crystalline domains in amorphous areas. (b) A Part of stacked $2DC_3N_3$ sheets and (c) related electron diffraction pattern. (d and e) HRTEM image of a $2DC_3N_3$ sheet with different magnifications. Stacked layers with 0.258 nm distance can be clearly seen in these images. (f) HRTEM of a $2DC_3N_3$ and related unit cell obtained by patterns in this image.

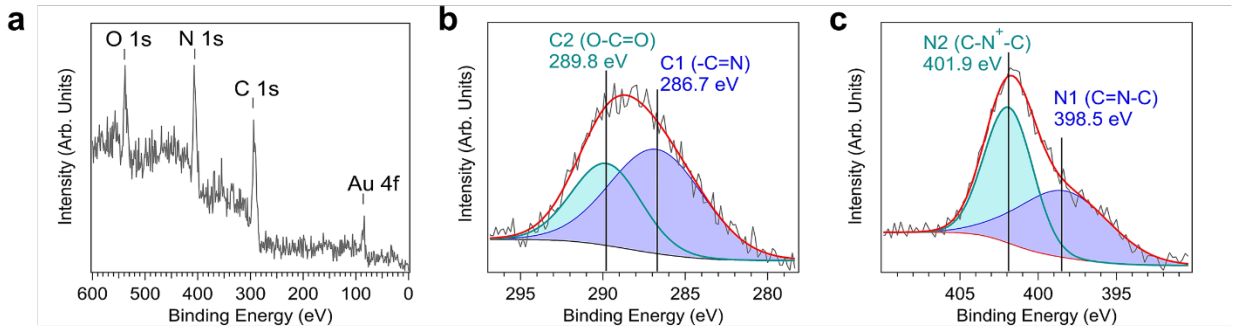

d

Elt	EDX %	EA %	XPS %	Expected %
C	41.44	35.42	47	46.16
N	38.08	34.17	35	53.84
O	20.48	-	17	-
H	-	2.88	-	-
C/N	1.08	1.03	1.34	0.85

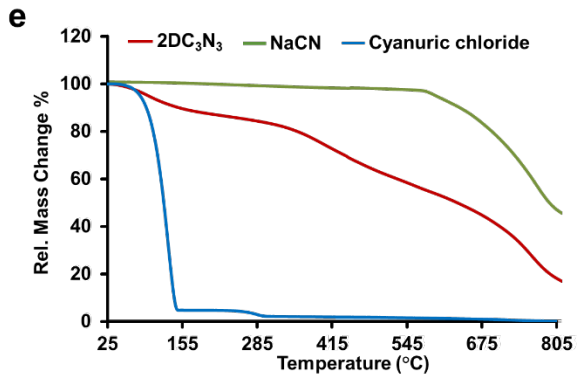

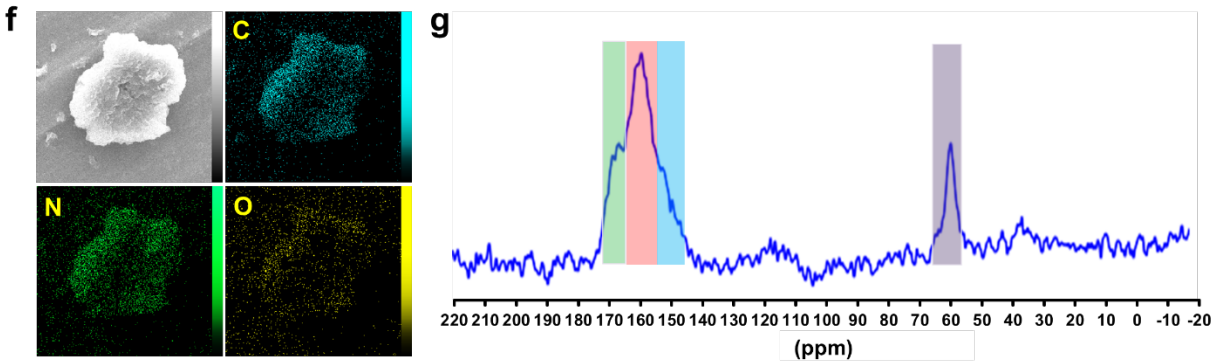

Fig. 3. (a) Survey, (b) highly resolved C1s and (c) highly resolved N1s spectra of $2DC_3N_3$. (d) Composition of $2DC_3N_3$ obtained by XPS, elemental analysis and EDX. (e) TGA thermograms of $2DC_3N_3$ and its precursors at a heating rate of 10 $^{\circ}C.\ min^{-1}$ under argon. (f) Mapping of $2DC_3N_3$ composition and carbon, nitrogen and oxygen element scattering pattern. (g) CP-MAS NMR spectrum of $2DC_3N_3$, showing distinguished signals for the triazine rings, methoxy and carboxyl functional groups.

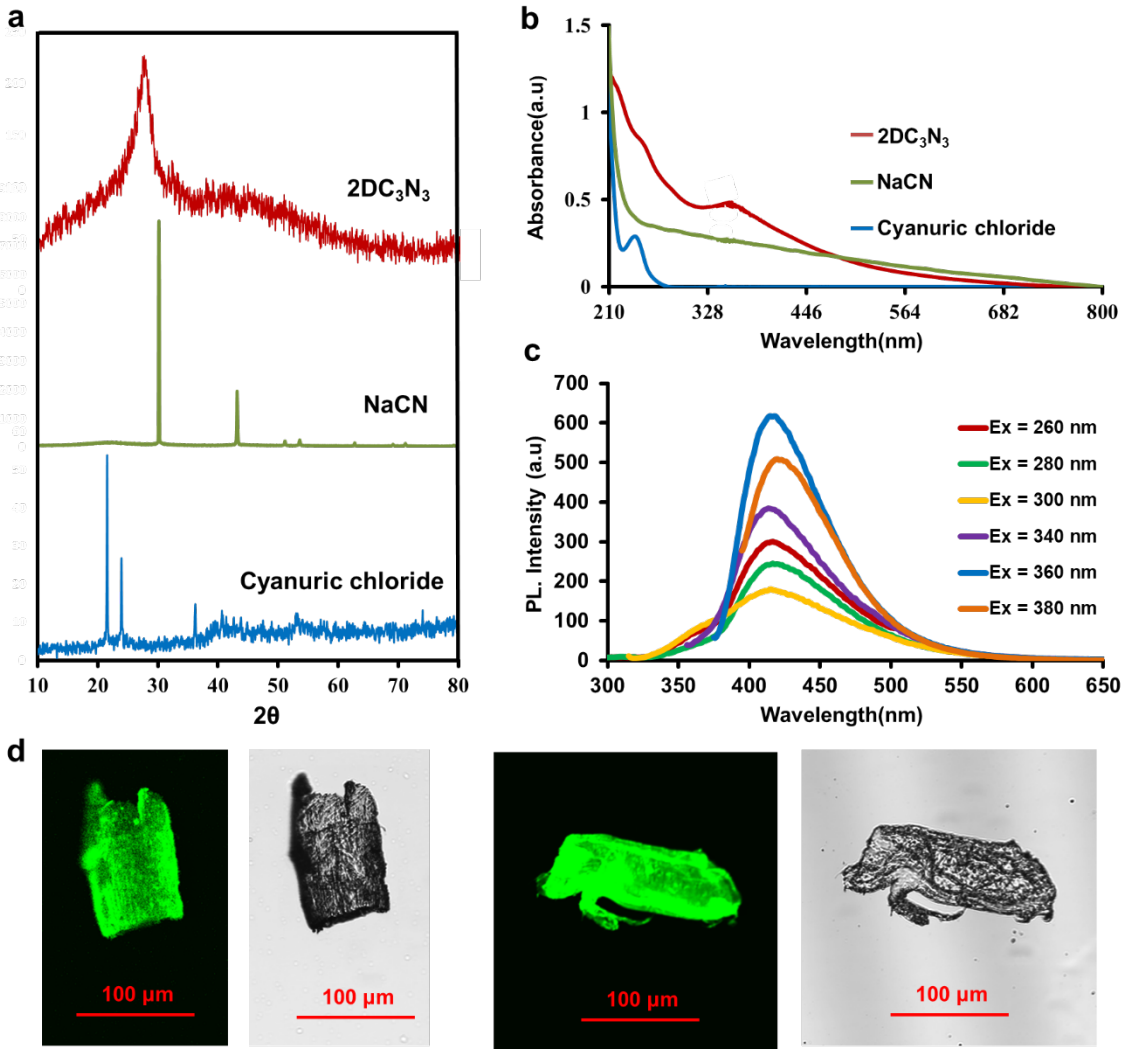

Fig. 4. (a) XRD diffractograms of $2DC_3N_3$ and its precursors. A sharp peak at 27.32° was assigned to the sheet-like structure and crystallinity of this compound. (b) UV-vis spectra of $2DC_3N_3$ (0.4 mg. ml^{-1}) and its precursors in (0.1 mg. ml^{-1}). (c) The photoluminescence (PL) spectra of $2DC_3N_3$ (0.5 mg. ml^{-1}) at different excitation wavelengths. (d) Confocal laser scanning microscopy (CLSM) image of individual $2DC_3N_3$ sheets. Sheets were excited by 405 nm wavelength.

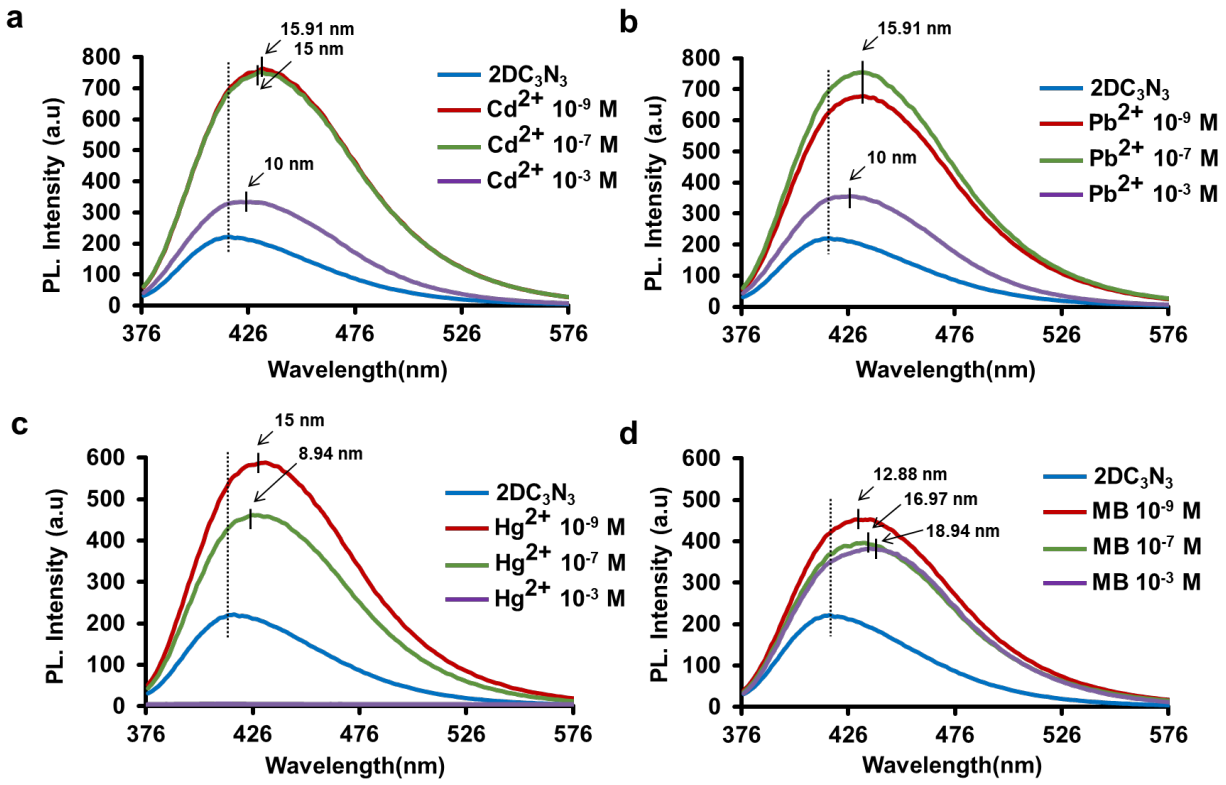

Fig. 5. The photoluminescence (PL) spectra of $2DC_3N_3$ (0.5 mg. ml^{-1}) in the presence of different concentrations of Cd^{2+} (a), Pb^{2+} (b), Hg^{2+} (c) and MB (d) at 360 nm excitation wavelengths. In each figure, shifting of the maximum emission wavelength of $2DC_3N_3$ upon addition different concentrations of metal ions and dye are shown.

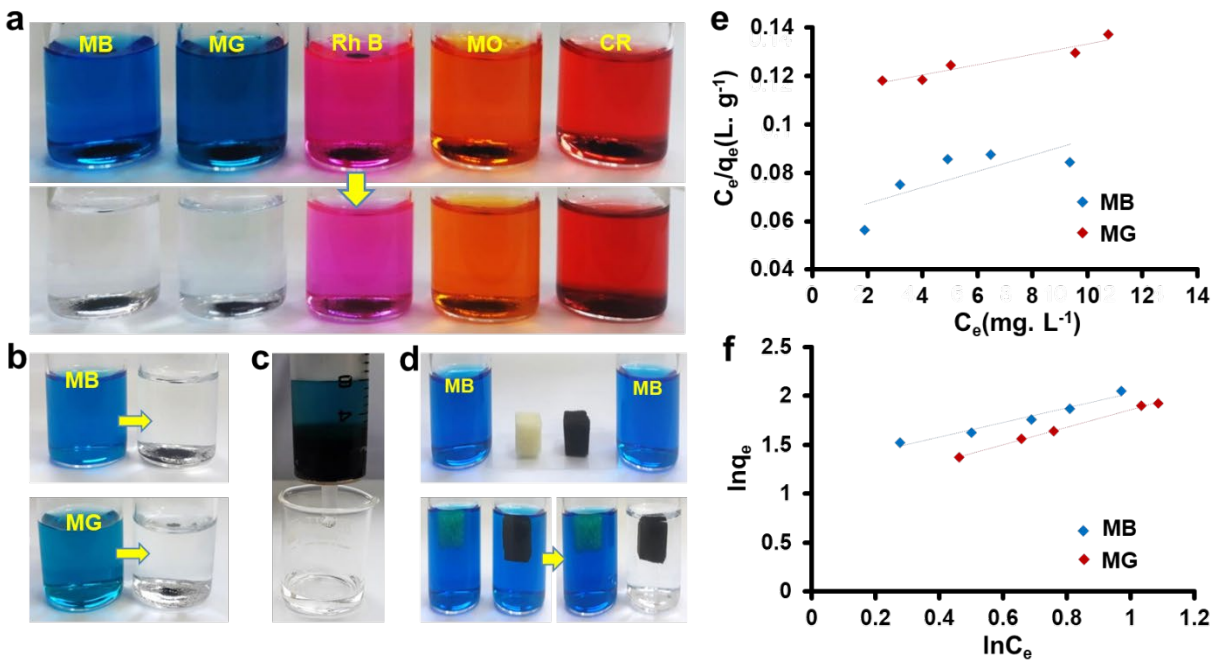

Fig. 6. (a) Incubation of water solutions of different dyes (20 mg. L^{-1}) with $2DC_3N_3$ after 1 min (upper row) and 120 min (bottom row). (b) Water solutions (20 mg. L^{-1}) of MB and MG before (left) and after (right) sonication with $2DC_3N_3$ (1 mg) for 120 seconds at room temperature. (c) Filtering a water solution of MB (20 mg. L^{-1}) by sponge-$2DC_3N_3$ and almost complete removal of dye from water. (d) Complete removal of MB (20 mg. L^{-1}) in 10 ml of water by cubic sponge-$2DC_3N_3$ after 120 min at room temperature without shaking. The white and black sponges are polyurethane sponges before and after treatment with $2DC_3N_3$. (e) Langmuir and (f) Freundlich adsorption isotherms of MB and MG by $2DC_3N_3$.

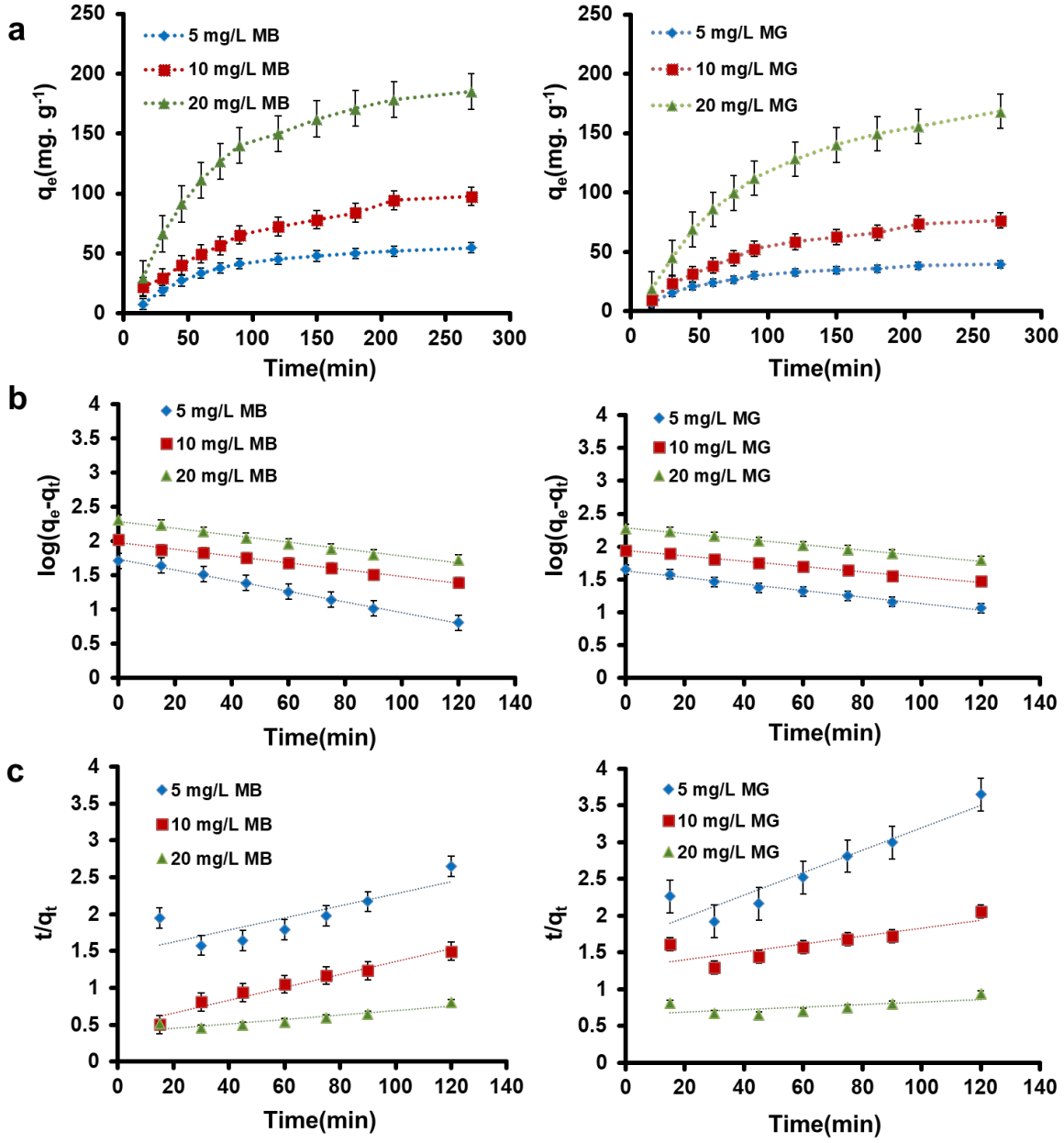

Fig. 7. (a) The effect of contact time on the adsorption capacity of MB and MG by $2DC_3N_3$. (b) Pseudo-first order and (c) pseudo-second order adsorption kinetic profiles for MB and MG by $2DC_3N_3$.

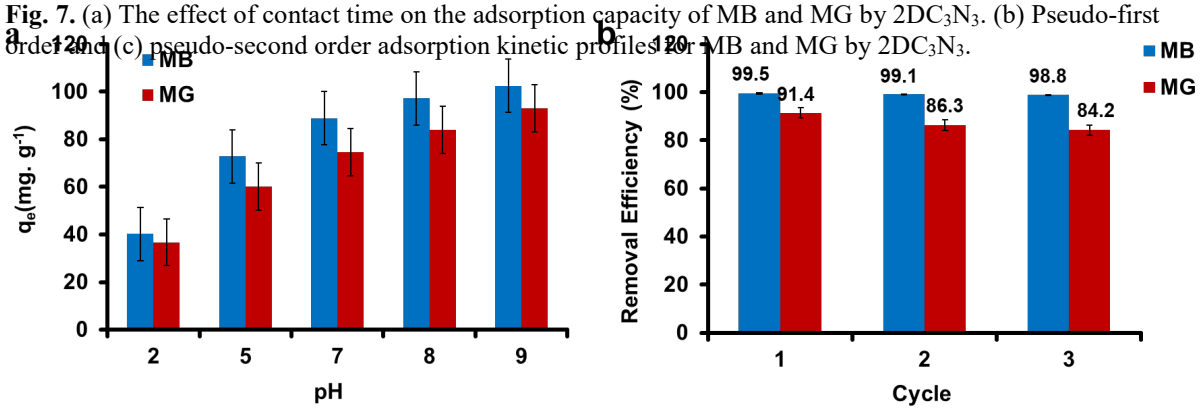

Fig. 8. (a) The effect of pH on the adsorption capacity of MB and MG by $2DC_3N_3$. (b) Reusability of the $2DC_3N_3$ for three successive adsorption-desorption cycles for MB and MG.